PAPER

Thermal oxidation synthesis of crystalline iron-oxide nanowires on low-cost steel substrates for solar water splitting

IOP Publishing Semiconductor Science and Technology
Semicond. Sci. Technol. 32 (2017) 084001 (10pp) https://doi.org/10.1088/1361-6641/aa7593

Thermal oxidation synthesis of crystalline iron-oxide nanowires on low-cost steel substrates for solar water splitting

T Dlugosch[1], A Chnani[1], P Muralidhar[1], A Schirmer[1], J Biskupek[2] and S Strehle[1]

[1] Ulm University, Institute of Electron Devices and Circuits, Albert-Einstein-Allee 45, D-89081 Ulm, Germany
[2] Ulm University, Central Facility of Electron Microscopy, Albert-Einstein-Allee 11, D-89081 Ulm, Germany

E-mail: steffen.strehle@uni-ulm.de

Received 31 March 2017, revised 17 May 2017
Accepted for publication 30 May 2017
Published 11 July 2017

Abstract

Iron-oxide and in particular its crystallographic phase hematite (α-Fe_2O_3) is a promising candidate for non-toxic, earth abundant and low cost photo-anodes in the field of photo-electrochemical water splitting. We report here on the synthesis of α-Fe_2O_3 nanowires by thermal oxidation of low-cost steel substrates. Nanowires grown in this manner exhibit often a blade-like shape but can also possess a wire-like geometry partly decorated at their tip with an iron-rich ellipsoidal head consisting also of crystalline iron-oxide. We show furthermore that these ellipsoidal heads represent suitable growth sites leading in some cases to an additional growth of so-called antenna nanowires. Besides nanowires also nanoflakes were frequently observed at the surface. We discuss the influence of the oxidation temperature and other synthesis parameters as well as dispute the current growth models. Finally, we show that our α-Fe_2O_3 nanostructures on steel are also photo-electrochemically active supporting in principle their use as photo-anode material.

Supplementary material for this article is available online

Keywords: photo-electrochemistry, solar water splitting, photo-anode, hematite nanostructure, hematite nanowire

(Some figures may appear in colour only in the online journal)

Introduction

Solar energy harvesting belongs undoubtedly to the most promising concepts to cope with an increasing global demand for energy and limited fossil resources considering also their inherent negative environmental impacts. Besides the possibility to extract electrical power from a solar cell that needs to be stored or transported with minimized losses, photo-generated charge carriers can also be utilized to drive electrochemical reactions in so-called photo-electrochemical cells (PECs). A fundamental PEC application is solar water splitting to generate hydrogen as an ultimate clean fuel itself or as a precursor for a CO_2 neutral ethanol fabrication [1]. The overall idea of PECs resembles the natural photosynthesis process [2] supporting its great appeal. However, several challenges need to be addressed in order to compete at the current stage with fossil energy generation and to act as a reliable energy generation strategy in the future [3].

An important part of a PEC is the so-called photo-anode providing photo-generated holes to oxidize water. It has been demonstrated in 1972 [4] that semiconductors, exemplary shown for TiO_2, can act as photo-anodes for water splitting applications. Since then numerous semiconducting materials such as WO_3 [5], MoS_2 [6], α-Fe_2O_3 [7, 8] and many more were studied accordingly. The iron-oxide phase α-Fe_2O_3 or hematite appears as a suitable and low-cost photo-anode

candidate and has therefore attained already much attention in the past (see [8]).

Hematite is a low-cost earth abundant, and non-toxic *n*-type semiconductor exhibiting an indirect band gap of about 1.9–2.2 eV depending on the synthesis method as discussed in [7]. The band gap allows therefore photon absorption in the desired visual spectrum starting at a wavelength of approximately 650 nm. Based on the band gap of hematite and thermodynamic considerations a theoretical maximum efficiency for solar-to-hydrogen conversion of 12.9% (AM1.5 solar illumination) has been reported [9], which is above the benchmark value of 10% [10] commonly assumed for commercial applicability. Also recent studies have shown that hematite appears to be stable under PEC water splitting operation and solar illumination [3, 11]. However, besides all these promising aspects, hematite shows some major drawbacks, as summarized for instance in [3, 7, 8] that must be addressed. At the forefront of these drawbacks is the low charge carrier lifetime of typically only a few picoseconds translating into a diffusion length of only a few nanometers that is in misalignment with an optical absorption depth of several hundred nanometers. Other drawbacks are the overall low charge carrier concentration that is for instance addressable by doping (e.g. Ti, Sn, Zn) as well as the large overpotential or slow charge transfer kinetics addressable by suitable surface modifications [7, 12]. For the synthesis of hematite, often as thin film [13], numerous strategies exist but nanostructuring is currently one of the key strategies to cope with the drawbacks of hematite as demonstrated initially for cauliflower-like nanostructures [14].

Here, a nanowire array is utilized as a so-called morphology strategy as discussed for instance before in [7]. Vertically aligned nanowires excelled in performance offering for instance a drastically increased electrode surface, important to drive the photoelectrochemical charge transfer [15]. The surface can also be further modified to lower the surface recombination rate or to promote the charge carrier transfer to the electrolyte. Additionally, photo-generated charge carriers need in principle only to traverse a few nanometers to reach the surface. Another advantage that comes along with a nanowire array strategy is efficient light trapping [15]. As nanowire arrays do not exhibit a well-defined interface but a gradual change in the air material ratio, the refractive index changes as well gradually. This lowers intrinsically the surface reflectivity and allows efficient light absorption along the nanowire axis, which are typically a few micron long. The enhanced light trapping in nanowire arrays was demonstrated for instance by 3D simulations elsewhere [16]. The use of α-Fe_2O_3 nanowire arrays has been already discussed before [15, 17] specifying nanowire diameters of 5–10 nm to support efficient hole transport to the surface and a nanowire length of at least 400–500 nm to absorb the incoming light completely within the array. With view to commercial applications, nanowire or nanostructure synthesis must also be realizable at low cost and with high reproducibility on a large scale. So far only few bottom-up techniques exist serving in principle this purpose (i) solution-based hydrothermal synthesis [18–21], (ii) electrodeposition [22], and (iii) thermal oxidation of iron [23–27]. That plain thermal oxidation of iron in air at elevated temperatures, as the method applied here, yields crystalline hematite nanowires and nanoflakes in a self-forming or catalyst-free manner is known since the mid 50s [23] and was also observed for other metals such as copper [28]. Considering the simplicity and effectiveness of this nanowire growth strategy it is rather surprising that only few papers dealt with this synthesis method since then compared for instance to the well-known vapor-liquid-solid growth of nanowires [29]. Besides ambient oxidation in air, nanowire growth from iron substrates was demonstrated for plasma oxidation [30] or oxidation in CO_2, SO_2, NO_2 [25, 26] or O_3 [31].

Also, direct electrical heating of an iron wire in ambient air yielded iron-oxide nanowires [32]. Nevertheless, studies are so far primarily focused on high-purity iron as a substrate material, contradicting a low-cost synthesis approach. Here, we examined therefore the formation of hematite nanowires, mainly in the temperature range of 300 °C–700 °C, by thermal oxidation of common inexpensive low-carbon steel sheets and achieved overall comparable results to high-purity iron considering also their photo-electrochemical activity. Based on the fact that nanowire growth is typically accompanied by the formation of various nanostructures, we also introduce a suggestion for a nanostructure categorization considering previous reports. Furthermore, hardly described nanolamellas and nanowires possessing a crystalline iron-rich ellipsoidal head as well as so-called antenna nanowires are shown. These observations shall also allow to further dispute and extent the existing growth models.

Experimental

For our experiments, low-carbon steel purchased as 0.15 m by 2.5 m roll with 200 μm in thickness (Precision Brand Products, Inc., steel shim stock low-carbon C1008/C1010) were used as substrate material. The maximum carbon content is specified with 0.13 wt%. Besides carbon, 0.3–0.6 wt% manganese, 0.04 wt% phosphorous and 0.05 wt% sulfur are present. Pieces of about 1 cm^2 were mechanically cut from the steel roll as substrate material and pre-cleaned in acetone and isopropanol, each for 5 min, with ultrasound support. The samples were successively etched in hydrochloric acid (32–36 vol%) for 90 s to remove the native oxide, providing a well-defined initial state, followed by a 60 s purge in deionized water to remove the acid. As also hydrogen may develop during the etching in reaction with iron, moderate sample agitation is recommended to release gas bubbles from the surface and to allow for a homogeneous etching of the entire surface. After the etching, the samples exhibit a homogeneous gray non-shiny finish and were placed immediately in the oxidation furnace. For the oxidation process a common horizontal quartz tube oxidation furnace (Thermco Products Corporation) was utilized. The samples were put on a ceramic holder and placed in the center of the quartz tube having an inner diameter of about 5.5 cm and a length of about 120 cm. The steel samples were oxidized in ambient air for typically

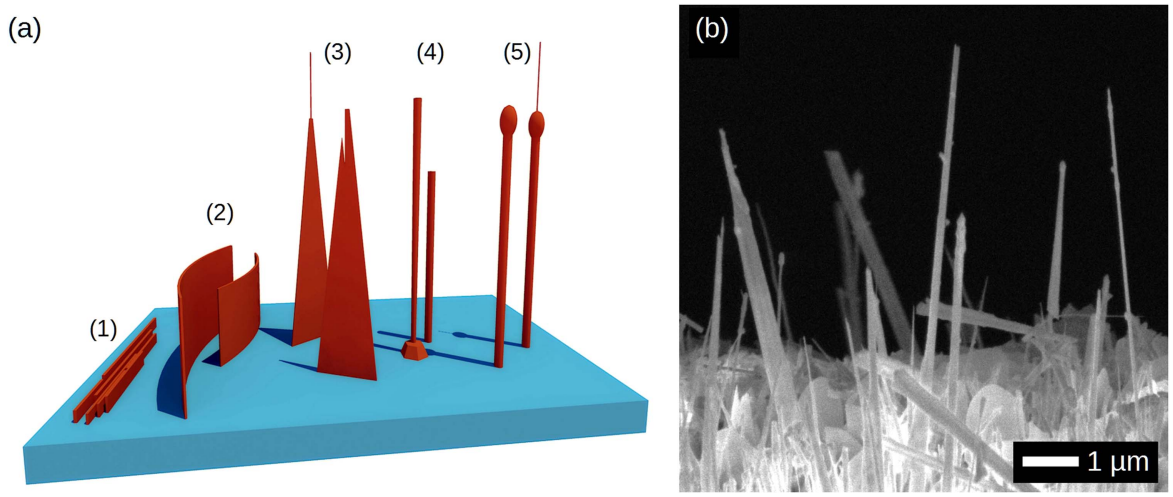

Figure 1. (a) Schematic illustration of the observed principle nanowire morphologies labeled as follows: (1) nanolamellas, (2) nanoflakes, (3) blade-like nanowires some with an antenna nanowire, (4) wire-like nanowires sometimes growing on a distinct base crystal, (5) wire-like nanowires with an ellipsoidal head and partly decorated with an antenna nanowire. Please notice that the drawing does not reflect the actual size ratios and that there are smooth transitions between the morphologies. (b) Representative SEM image of an annealed steel sheet (620 °C for 2 h in air) showing several nanostructure morphologies but lacking morphologies of type (1).

0.5–2 h and at temperatures of 300 °C–1000 °C (typically 600 °C–700 °C) using heating rates of maximum 25 K min^{-1}. Scanning electron microscopy (SEM) was carried out using mainly a Leo Zeiss 1550 applying the inlens secondary electron detector for imaging. Transmission electron microscopy (TEM) to characterize the crystal structure, morphology and composition on the nanoscale was done using a Philips CM20 operated at 200 kV equipped with a CCD camera for imaging and EDX system (EDAX) for elemental analysis. Prior to the TEM investigations, the nanowires were mechanically removed from the substrate and suspended in isopropanol by gentle ultrasound treatment and drop casted onto lacey carbon grids. For the photo-electrochemical characterization of hematite nanowires a potentiostat from Princeton Applied Research (PARSTAT2273) equipped with a XBO 75 W/2 xenon short-arc lamp for illumination was used and operated with a scan rate of 20 mV s^{-1}. The samples were placed in a 1 M NaOH electrolyte using a three-electrode cell with a Luggin capillary saturated calomel electrode (SCE) as reference electrode and a Pt wire acting as counter electrode.

Results and discussion

The thermal oxidation of iron and steel substrates yields commonly not a fully homogeneous set of nanowires but results frequently in various nanostructure morphologies emerging in parallel as shown in figure 1. Besides wire-like and blade-like nanowires, also nanolamellas and nanoflakes can be observed. As it will be described in greater detail in the following, some nanowires exhibit an ellipsoidal head at their tip that can supported in some cases another nanowire with smaller diameter. This particular morphology was not described for hematite nanowires so far to the best of our knowledge. The different morphologies are illustrated schematically in figure 1(a) and are also shown in the SEM image given in figure 1(b) except for the nanolamellas (see figure 3(c)). The dominating morphology or the frequency of a certain kind of nanostructure appears to be dependent on the growth conditions such as temperature, oxygen partial pressure, surface dislocation density, surface cleanliness and gas flow (e.g. [33]).

Furthermore, Srivastava *et al* [34] showed that also the substrate texture was influential in their experiments, which should contribute to the so far limited reproducibility or inhomogeneity of the nanowire growth. However with respect to the application, there is currently no distinct preference for a certain kind of morphology as all hematite nanostructures should roughly represent in principle the desired properties specified before [15, 17].

The growth model for the catalyst-free formation of hematite nanowires is still incomplete but dates back in its fundamental principle already to the mid 50s [23]. Takagi [23] described tip-growth of the nanowire or thickening if the tip sites were blocked by contamination leading to the assumption that surface diffusion and crystallization at preferred crystal facets are the main driving forces. Yuan *et al* [35] used in their nanowire growth experiments at 400 °C–600 °C 99.99% pure iron foils and extended the model by compressive stress relaxation as a consequence of the surface oxidation causing directed grain boundary and surface diffusion. Other mechanisms, as also summarized in [23, 35], consider also diffusion through internal channels, represented for instance by the core of a screw dislocation, or nanowire growth due to evaporation and condensation of species. While the latter one was already discarded in the mid 50s [23] with respect to the melting point of iron, dislocation supported diffusion for nanowire growth, as for instance described by Tallman *et al* [24], might still be an important aspect as also briefly discussed in the following.

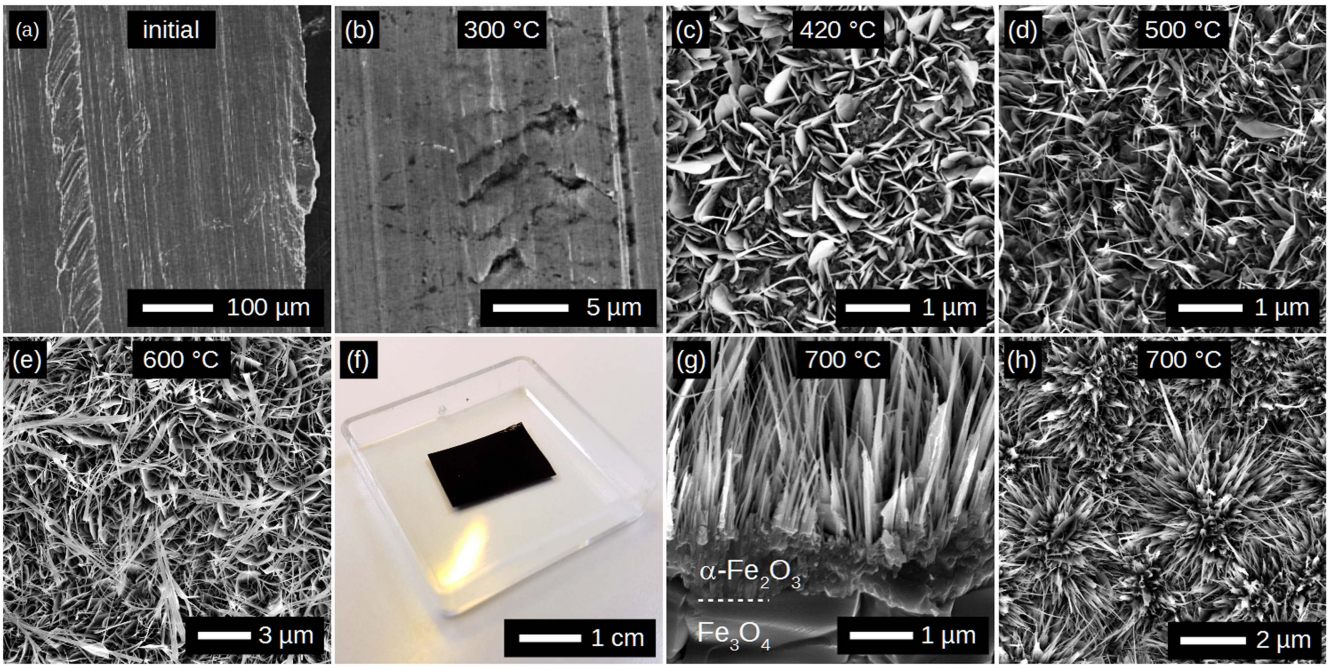

Figure 2. (a) The initial state of the steel surface is shown exhibiting clearly grooves and scratches. (b) After 300 °C annealing in air for 2 h no significant changes were observed with respect to nanowire growth. (c) Annealing at 420 °C for 2 h yields the first nanostructures consisting predominately of nanoflakes and only few scattered nanowires. (d) An increase to 500 °C for 2 h increased the number of hematite nanowires significantly. Both, short blade-like nanowires and longer wire-like nanowires are observable. (e) Nanowire elongation and a dense coverage with nanowires and nanoflakes is observed for an annealing at 600 °C for 2 h. (f) Macroscopic image of the sample after an oxidation at 650 °C showing the black velvet-like appearance with a slight red–brownish color cast. (g) The well-known top hematite layer and the magnetite layer underneath are clearly visible and indicated in the SEM cross-section of a sample annealed at 700 °C for 2 h. (h) Top-view of a steel sample oxidized at 700 °C for 1 h. The floral-like arrangements of the nanowires can be seen.

Aiming for a low-cost hematite nanostructure synthesis it is rather surprising that to the best of our knowledge so far steel was not considered as an inexpensive substrate material in lieu of high-purity iron although steel can basically also consist of about 99 wt% pure iron. A contribution examining the effect of a substrate alloying element with respect to hematite thermal nanowire growth is given by Chueh *et al* [36] using $Fe_{0.5}Ni_{0.5}$ and $Fe_{0.64}Ni_{0.36}$ foils as substrate material. Their motivation for adding Ni had been the fact that the iron self-diffusion should be enhanced and therefore presumably nanowire formation, which had been accordingly observed in their experiments. Notably, Ni was effectively trapped in a $(Fe,Ni)_3O_4$ layer formed during the oxidation process such that the resulting α-Fe_2O_3-nanowires had been free of any detectable Ni contamination. For our steel sheets used here as substrate material, manganese is the impurity with the highest content but only with a concentration of up to 0.6 wt% as mentioned in the experimental section. Manganese could potentially segregate to the surface and be incorporated into the growing nanowires or affect their nucleation. However, an incorporation of manganese can be also considered as a beneficial aspect following a report from Gurudayal *et al* [20] who observed an improvement of the photo-current density by a factor of three and also a slight reduction of the water splitting onset potential due to Mn doping of solution-synthesized hematite nanorods.

The initial state of the pre-cleaned steel substrates is shown in figure 2(a) also illustrating evidently the plain surface quality indicated by the grooves and overall surface roughness. Annealing at 300 °C for 1–2 h did hardly trigger nanowire growth (figure 2(b)). Due to the low temperature, iron cation surface diffusion should be significantly suppressed. However, experiments done with sputtered iron thin films showed evidently that extended oxidation times of 24 h rather than 1–2 h can still yield some nanowires using temperatures as low as 255 °C [37] diminishing the necessity of compressive stress for a hematite nanowire growth.

If the steel substrates are annealed at 420 °C for 2 h as shown in figure 2(c), the substrate is fully covered with nanostructures that consist here primarily of nanoflakes with only few nanowires having a length of only a few hundred nanometers with the longest nanowires in the range of one micron. This correlates well with [33] but is different to Yuan *et al* [35] who observed mainly nanowires in low density. Chueh *et al* [36] showed that annealing at 400 °C with extended annealing time of 10 h yields also increased nanowire densities but strongly depending on the gas flow. This exemplifies already that the thermal oxidation method itself is overall robust but the growth, especially at lower temperatures, is intimately linked to experimental parameters such as set-up, flow rate, substrate material or sample pretreatment demanding further studies. In general, the nanoflakes appear about 5–50 nm thick and with a height and width of about 1–2 μm and about 1–10 μm, respectively. As for instance pointed our by Tallman *et al* [24], their thickness varies hardly with their width. Nanowires and nanoflakes can grow

in separated areas but are more often intermixed. If annealing is realized at 500 °C for 2 h, more nanowires were observed consisting of blade-like and wire-like nanowires (figure 2(d)). If the annealing time is reduced to only 0.5 h nanowires were hardly observed at the surface anymore.

If the annealing temperature is further increased to 600 °C nanowires get longer, typically about 2–6 μm, and more blade-like nanowires appear that could maybe result also from merged wire-like nanowires (figure 2(e)). The macroscopic sample appearance will also change in dependence of the nanostructure coverage or the annealing temperature from a metal-gray finish at the beginning over a red–brownish color to an almost black velvet-like appearance with only a slight red–brownish color cast for high nanowire densities as shown in figure 2(f). A further increase of the temperature to 700 °C does not result in a significant change of the overall surface morphology as shown in figure 2(g) but yields typically longer nanowires partly up to 12 μm, which is in agreement with Takagi [23]. In dependence on the observation perspective floral-like arrangements of the nanowires can be also observed frequently (figure 2(h)) that might originate from the initial microstructure of the substrate. In general, nanoflakes appear to be present more often at the rim of the sample in a stacked manner. If the annealing temperature is further increased no significant change was observed until 800 °C, whereas at 1000 °C the sample starts glowing and no nanostructures were detected anymore at the surface. Also Takagi [23] reported an optimal nanowire nanowire growth in the temperature range of 600 °C–700 °C and also a linear relationship of nanowire length and annealing time. However, we observed overall only a moderate increase in the nanowire length between an annealing of 1–2 h. It must be generally mentioned that the oxide surface layers formed at the steel surface during annealing are highly brittle and can easily detach from the buried iron. This is a major drawback for the use of bulk iron or steel, commonly not highlighted, for any application suffering from potential mechanical impacts onto the surface comprising also the targeted photoelectrochemical water splitting. Here, further strategies in synthesis have to be developed to tackle this issue effectively. The origin of the brittleness is the built-up of compressive stress during the surface oxidation leading to the formation of multiple oxide layers (see figure 2(g)) for the surface region. As examined in detail for pure iron [32], these layers of iron-oxide consist from iron to the top of the stable iron-oxide phases wustite (FeO, *p*-type semiconductor with 2.3 eV band gap [38]), for annealing temperatures above 600 °C, followed by magnetite (Fe_3O_4, *n*-type semiconductor with almost metallic conductivity, band gap 0.1 eV [38]) and finally of a hematite layer decorated with the hematite nanowires (see supplementary information S1 is available online at stacks.iop.org/SST/32/084001/mmedia: SEM/EDX of the top layer). The built-up of compressive stress in this layer stack was considered for instance by Mema *et al* [28] for CuO nanowire growth and by Yuan *et al* [35] to be an important driving force for the nanowire growth as mentioned before.

In order to study the initial nanowire formation, the annealing time has been reduced to only 0.5 h for an annealing temperature of 600 °C and above. Hence, only a partial coverage of the sample surface with nanostructures is obtained. Besides some blade-like nanowires and several nanoflakes, nanowires exhibit at several locations an ellipsoidal head already in their initial growth stage as evidently depicted in figure 3(a). The heads appear brighter than the nanowire itself, which could be caused by the particles volume but more likely by the effective mass meaning higher iron concentrations. Furthermore, the hematite top-layer appears like a porous network similarly observed in [33] for an annealing at 700 °C but lacking nanowires. At this point one might speculate whether the heads represent a catalyst and whether it originates from the hematite top layer or not. In other locations, small-diameter wire-like nanowires (figure 3(a) inset) seem to grow on top of a crystal that appears to represent a trigger point.

However, further studies are required to fully elucidate the growth mechanisms. If the growth time is extended, nanowires exhibiting an ellipsoidal head can be found frequently as for example shown in figure 3(b). Whether these ellipsoidal heads are equal to the heads observed during the initial growth stages, as shown in figure 3(a), is still unknown but might be given.

To the best of our knowledge only Wang *et al* [39] described an ellipsoidal head decorating the tip of α-Fe_2O_3 nanowires before. In their experiments they annealed iron samples with a purity higher than 99.96 wt% at temperature of 550 °C–600 °C using an oxidation time of several days and an oxidizing gas mixture of CO_2, N_2, SO_2 or H_2O vapor. Interestingly, they reported that most of their nanowires were exhibiting the ellipsoidal head after the growth, which seems not to be the case in our experiments. Experiments reported elsewhere do not provide evidence of such nanowires with an ellipsoidal head [32–36]. The main finding in [39], using comprehensive TEM studies, is that the crystalline ellipsoidal head resembles an iron-rich bi-crystal with a central twin plan decorating a bi-crystalline hematite nanowire. They speculate that this could be a bi-crystalline Fe_3O_4 precursor crystal yielding also the well-known bi-crystalline α-Fe_2O_3 nanowires. Accordingly, also single-crystalline nanowires were found in their experiments but lacking any head at the nanowire tip. In our experiments, nanowires exhibiting an ellipsoidal head were predominately observed in the vicinity to the samples rim indicating that possibly stress relaxation at the edges, higher surface defect concentrations, potentially induced by cutting the sample, or temperature gradients might contribute. In general, also gradients in the precursor concentration, here represented by oxygen, can be discussed. However, considering the small sample size of about 1 cm^2 in comparison to the furnace volume as well as the oxidation at ambient pressure using a non-sealed system, we currently believe that this effect should be of minor importance. Reasons why the head is only present in some cases have to be found in future studies. Another unique observation made partly is the growth of small-diameter nanowires, so-called antenna nanowires, out of these ellipsoidal heads as shown in figure 3(c). Also shown in figure 3(c) are nanolamellas present at the ground. The existence of antenna nanowires might

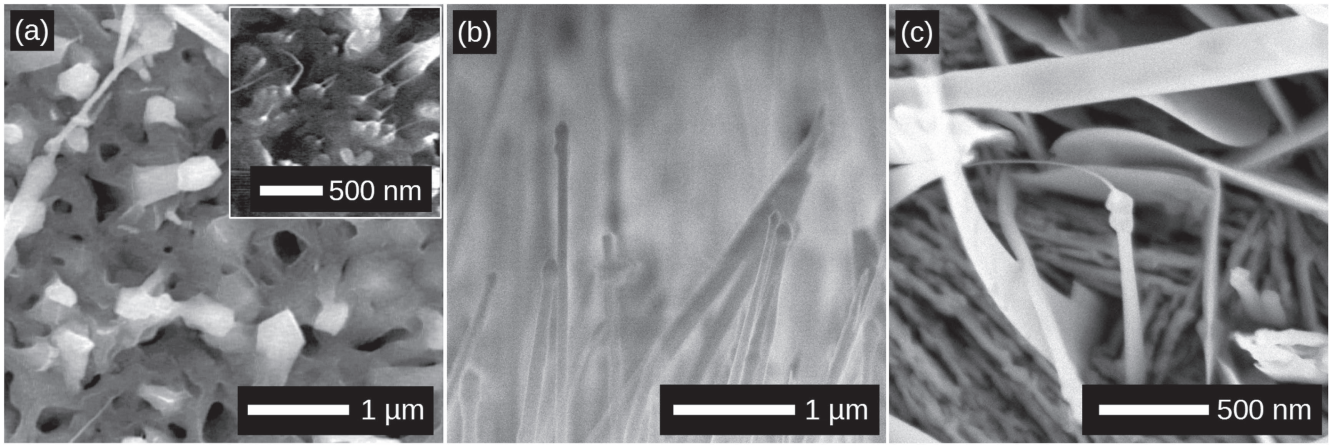

Figure 3. (a) Initial growth stages of nanowires after annealing at 600 °C in air for 0.5 h. Notably, many short nanowires exhibit at this stage an ellipsoidal head. Besides these nanowires with an ellipsoidal head also blade-like nanowires and nanoflakes were observed (not shown). The inset depicts wire-like nanowires growing from certain trigger points. (b) Some nanowires still possess after extended annealing of 1–2 h at 600 °C–700 °C an ellipsoidal head as also described by Wang *et al* [39]. (c) The ellipsoidal head can also serve as a support for another nanowire with much smaller diameter, which has been so far not highlighted in other reports. Furthermore, nanolamella formation can be seen at the ground.

imply a self-catalytic nature of these ellipsoidal heads or at least a trigger point capability for the nucleation of hematite nanowires most likely by surface diffusion. A question arising at this point is, whether these antenna nanowires grow at first, simultaneously or after the supporting nanowire is fully developed.

So far, it remains unclear if the antenna nanowires observed in figure 3(a) (inset) represent the antenna nanowires shown in figure 3(c) or if they grow at lower temperature for instance during the cooling down phase similar to observations made by Takagi [23] for the growth of small-diameter nanowires on blade-like nanowires. However, if samples were directly taken out of the furnace to quench the oxidation process, still some nanowires with ellipsoidal heads and few antenna nanowires were observable although their overall frequency appeared significantly reduced. TEM studies confirmed that nanowires grown on steel sheets consist also of the well-known bi- and single-crystalline hematite nanowires (see supplementary information S2). However, the blade-like nanowire laying on top of a bi-crystalline nanowire as shown in figure 4(a) seems to consist at its based of three single-crystals that might have merged during growth and that could potentially result from individual nucleation events reasoning their varying length. Furthermore, one of these crystals passes into a single-crystal hematite nanowire with smaller diameter (figure 4(a)). Again, these nanowires could be comparable in their growth to the antenna nanowires but could evolve also at lower temperature for instance during the cooling down phase [23]. In general, all nanowires observed were crystalline as for example shown in figure 4(b) for a single-crystalline wire-like nanowire lacking an ellipsoidal head. The presence of an ellipsoidal head however does not seem to indicate bi-crystals contrary to Wang *et al* [39]. An example for this is given with the images depicted in figures 4(c) and (d) showing different segments of the same nanowire. As depicted in the TEM bright- and the corresponding dark-field image in figure 4(c), a nanowire can consist at its base of a bi-crystal and continue as single crystal (indicated by an arrow in figure 4(c), top image). This appears in principle similar to the observation made in figure 4(a) but without the nucleation of an antenna nanowire. Notably for this nanowire, the single-crystalline segment exhibits at the tip an ellipsoidal head as shown in figure 4(d). This ellipsoidal head seems to lack a central twin plane but consists in agreement with [39] as well of crystalline iron-oxide. A magnified image of the head is shown in figure 4(e) with lattice fringes clearly visible. Here one may speculate whether the bi-crystalline nature of an ellipsoidal head can get lost leading to a transition from a bi- to a single-crystalline morphology during nanowire elongation. However, it appears at the current stage more likely, that a second nanowire nucleation event occurred. This second nanowire grows along the first single-crystalline nanowire possessing the ellipsoidal head, as similarly discussed before for a tri-crstalline hematite nanowire formation (see figure 4(a)). Nevertheless, also ellipsoidal heads with a central twin plane triggering bi-cystalline nanowire growth were found in support of [39] as shown in figure 4(f). Furthermore, TEM/EDX could confirm the iron-rich nature of the ellipsoidal heads (supplementary information S3) although the stability of such a phase in an oxidizing environment is still unclear. An example of an antenna nanowire growing out of an ellipsoidal head is shown in figure 4(g). As discussed before, further detailed studies are required to fully elucidate the underlying growth mechanisms but tip-growth as suggested by Takagi *et al* [23] appears so far still most suitable.

Besides surface diffusion, so far unspecified surface defects may assist nanowire nucleation. A method triggering the growth of small diameter nanowires while suppressing floral arrangements and nanoflake growth appears to be mechanical surface treatment causing for instance dislocations. Yuan *et al* [40] used in their experiments with pure iron conventional sandblasting to create a mechanical impact onto the surface. They observed that samples treated with

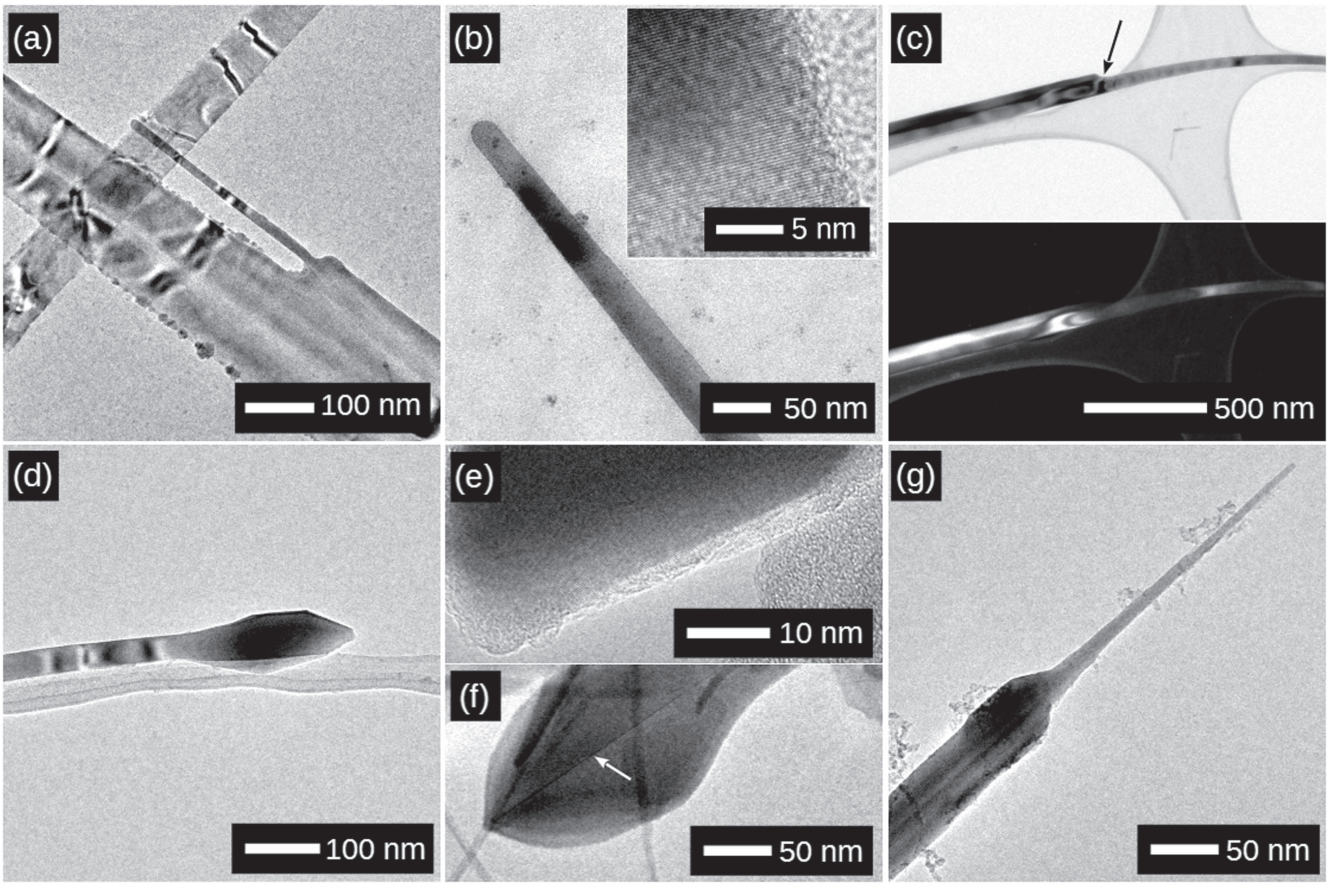

Figure 4. (a) Blade-like nanowire that appears to consist of three crystals at its base and continues to grow as a bi-crystal while the terminated part supports another single-crystal nanowire with smaller diameter. (b) Single-crystalline wire-like nanowire. The inset illustrates lattice fringes indicating the crystallinity. (c) Bright- (top) and a corresponding dark-field image (bottom) of a nanowire being bi-crystalline at its base and single crystalline at the tip. The transition area is indicated with an arrow. (d) The tip of the single-crystalline nanowire depicted in sub-figure c, which is decorated with an ellipsoidal head lacking any observable central twin plane. (e) Magnified area of the ellipsoidal head shown in sub-figure d indicating the crystallinity shown by the lattice fringes. (f) Ellipsoidal head with a central twin plane that nucleates a bi-crystalline nanowire. (g) Nanowire with ellipsoidal head decorated with a so-called antenna nanowire with small diameter.

sandblasting showed initially a higher nanowire density. Extended treatment however yielded more nanoflakes. In a straightforward attempt to examine the general influence of a mechanical impact or plastic surface deformation in our experiments, the steel sheets were locally deformed simply by using a conventional steel hammer as an effective tool. The sample was placed on a steel plate and flattened by hammering onto it, which induced local plastic surface deformations. Prior to the oxidation, the samples were cleaned as described in the experimental section. As a result, densely packed small diameter nanowires were observed within these local deformation areas (figure 5). This rough but effective strategy might be usable as well, but applied in a more controlled manner, to increase the yield of a certain kind of nanostructure during the oxidation and might help to elucidate the growth mechanisms further. Similar effects were observed if the surface was scratched using a hard steel needle. Notably, simple multiple bending did not enhance the nanowire growth but ongoing experiments using simple sandpaper pretreatment appeared to improve the nanowire nucleation even at lower temperatures of 300 °C. At this point it is worth noticing that also the storage time after cleaning effect the

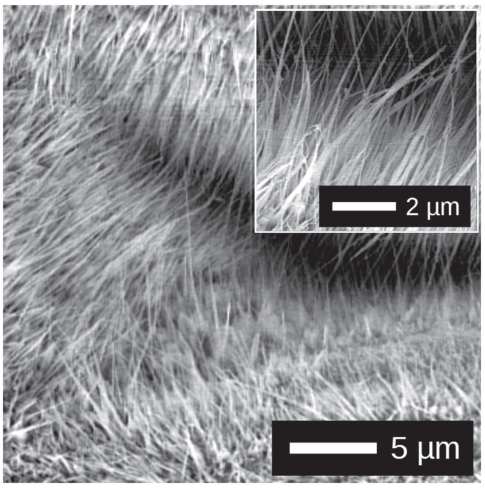

Figure 5. In areas of local plastic deformation, induced mechanically for instance here by hammering using a conventional hammer. Higher densities of nanowires were observed in plastically deformed regions compared to the surrounding while other morphologies such as nanoflakes were hardly detected. The steel sample depicted here had been annealed at 640 °C for 1 h. The inset represents a magnified image from the deformation area.

nanowire growth. Without presenting quantitative results, if pre-cleaned steel samples were stored for more than two days in ambient air, the nanowire density seemed to decrease in favor of nanoflakes. Also the overall homogeneity appeared decreased, which was also the case if the hydrochloric etching step was not done. Differences in surface quality prior to oxidation contribute most likely significantly to the observed differences in nanowire densities and occurring morphologies besides the general synthesis parameters.

In the last section of this paper, some properties with respect to the targeted application of photo-electrochemical water splitting shall be presented. As several authors have discussed (e.g. [3, 8]), pristine hematite regardless of its morphologies seems not to show great promise unless the drawbacks discussed before are tackled satisfactory. In this regard, the incorporation of the manganese as the alloying element with the highest concentration could be a promoter for the photo-electrochemical activity as already mentioned [20]. TEM/EDX studies did however not reveal, within the detection limit (approximately 0.5 at%), the presence of any manganese in the nanowires. Similar to the growth of pure hematite nanowires on iron-nickel alloy substrates [36], manganese might get trapped in the formed oxide layers underneath the nanostructures. In this context, Wang *et al* [39] reported that also gas phase impurities like sulfur that could potentially lead to iron-sulfur compounds like pyrite (FeS_2) were not incorporated. Therefore, effective strategies of doping must be developed for hematite nanowires obtained by thermal oxidation to utilize these structures as efficient photo-anodes in PEC. To examine the photo-electrochemical performance in general, cyclic voltammetry measurements using a common three electrode configuration were done with and without illumination for a steel sample oxidized at 620 °C for 1 h (see supplementary information S4). The hematite sample acts here as photo-anode or so-called working electrode, a Pt wire represents the counter electrode or cathode, and a SCE provides a stable potential reference to determine or control the voltage change. As shown in figure 6 a bias of about 0.53 V versus SCE is required without illumination (dark) to induce water splitting or so-called electrolysis. Considering the ideal water splitting potential and over-potentials the voltage between working and counter electrode should be higher than 1.23 V [4]. The photo-generation of charge carriers or in particular the holes in the hematite would not only change the surface potential but promote the probability of a charge transfer or water splitting. If the hematite photo-anode is illuminated an increase in the measured current, in comparison to the dark current, is observed at a voltage of about 0.02 V versus SCE. This represents a shift for the water splitting onset of almost 0.5 V versus SCE towards lower voltages due to illumination indicating the photo-electrochemical activity of our hematite nanostructures grown on low-carbon steel sheets. This result agrees well with the observations shown in [33] for thermally grown hematite nanowires on high-purity iron supporting our low-cost approach. Nevertheless, the overall voltage shift and the moderate current increase due to illumination are still too low to allow efficient water splitting. Besides an increase in the

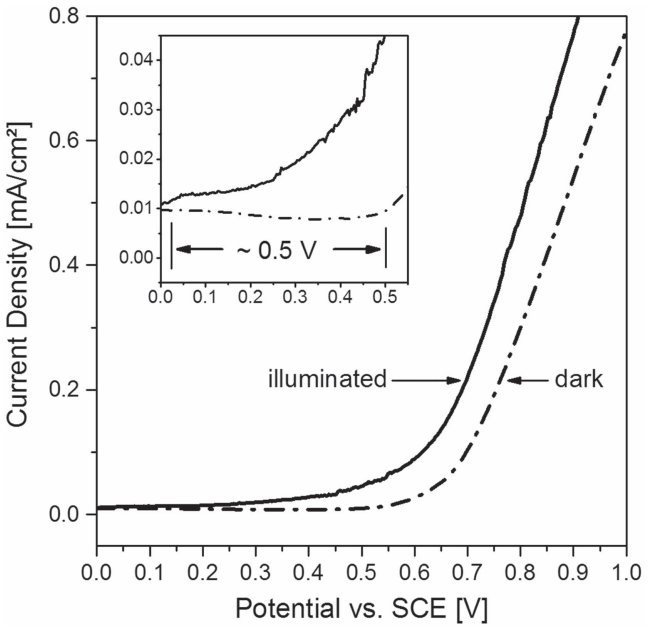

Figure 6. Cyclic voltammetry of a hematite nanowire sample annealed at 620 °C for 1 h. Shown is the forward scan without (dark) and with illumination. For the measurement a saturated calomel electrode (SCE) was used as reference electrode. If illumination is applied a shift of the anodic current onset for water splitting by almost 0.5 V is observed. The inset provides a magnified plot of the lower potential region. The SEM image depicting the surface of this sample is shown in the supplementary information S4.

light intensity and the already above discussed strategies and requirements to improve the photo-electrochemical performance of hematite for instance by doping, co-catalysts, improved charge carrier separation and reduced surface recombination, the specifics of our hematite sample must be considered here as well. So far the influence of the oxide layers forming on steel (e.g. $Fe/FeO/Fe_3O_4/Fe_2O_3$) on the charge carrier transport and the overall electrical contact is unknown. However, more detailed studies to examine the photo-electrochemical properties are required but ongoing.

The oxidation of steel or iron represents definitely an interesting and promising strategy for a low-cost and straightforward nanostructuring by the synthesis of crystalline hematite nanowires and other nanostructures. The roughly vertically aligned nanowires enable an efficient light coupling, and the large surface area supports not only efficient charge transfer to the electrolyte but also efficient surface modifications. Existing strategies to enhance the photo-electrochemical performance such as co-catalysts [41], Al_2O_3 coatings [42] or gold nanoparticles to exploit plasmonic effects [43] can be readily applied. Nevertheless, the understanding of the underlying growth mechanisms is still insufficient to assure controlled and reproducible synthesis. Further examination of the antenna nanowire being partly present on top of the ellipsoidal heads or *in situ* studies of the initial growth stages should provide valuable insights into the synthesis and growth of hematite nanowires. More precise growth models are also required to lower the growth temperatures further, address the brittleness of the surface and

enable efficient doping strategies as well as control over the synthesis of a particular nanostructure like nanoflakes, wire-like or blade-like nanowires. Also, the transfer of thermal oxidation nanowire synthesis to other materials and substrate systems would benefit to unleash the full potential of this kind of nanowire synthesis strategy.

Conclusion

We have shown that hematite nanowires can be grown by simple thermal oxidation in air at elevated temperatures using plain low-carbon steel sheets as substrate material rater than high-purity iron. From the growth experiments, multiple morphologies of nanostructures were observed including the well-known blade-like and wire-like nanowires as well as nanoflakes and sometime nanolamellas. The experiments showed that some nanowires possess an iron-rich ellipsoidal head consisting as well of iron-oxide that supports in some cases another nanowire with smaller diameter. These so-called antenna nanowires were to the best of our knowledge not reported before. Manganese as a substrate alloying element could not be detected in the hematite nanowires. We discussed furthermore that mechanical surface deformation, for instance by plain hammering, appeared to improve the yield of small-diameter and long nanowires while suppressing nanoflake formation. Experiments to demonstrate the photoelectrochemical activity showed finally that the hematite nanowires grown on steel are also photo-active and comparable to nanowires grown on high-purity iron. The measurements showed a shift due to illumination of almost 0.5 V versus SCE for the water splitting onset towards lower potentials. Steel represents consequently a low-cost substrate material for the thermal oxidation synthesis of hematite nanostructures. However, more detailed studies are required to elucidate the growth mechanisms, to develop a unified model explaining the different morphologies and to finally enable rational control of the thermal oxidation synthesis of hematite nanowires.

Acknowledgments

The authors thank A Schreiber, A Minkow, S Jenisch, R Ehrlich, A M Steinbach, T Diemant, and R Zeller from Ulm University (Ulm, Germany) for supporting the experimental work as well as T Cohen-Karni from Carnegie Mellon University (Pittsburgh, USA) for the inspiring discussion about the ellipsoidal nanowire heads.

References

[1] Highfield J 2015 Advances and recent trends in heterogeneous photo(electro)-catalysis for solar fuels and chemicals *Molecules* **20** 6739–93
[2] Barber J 2009 Photosynthetic energy conversion: natural and artificial *Chem. Soc. Rev.* **38** 185–96
[3] Tamirat A G, Rick J, Dubale A A, Sub W-N and Hwang B-J 2016 Using hematite for photoelectrochemical water splitting: a review of current progress and challenges *Nanoscale Horiz.* **1** 243–67
[4] Fujishima A and Honda K 1972 Electrochemical photolysis of water at a semiconductor electrode *Nature* **238** 37–8
[5] Liu Y, Li Q, Gao S and Shang J K 2014 Template-free solvothermal synthesis of $WO_3/WO_3{\cdot}H_2O$ hollow spheres and their enhanced photocatalytic activity from the mixture phase effect *Cryst. Eng. Comm.* **16** 7493–501
[6] Pan J, Wang Z, Chen Q, Hu J and Wang J 2014 Band structure engineering of monolayer MoS_2 by surface ligand functionalization for enhanced photoelectrochemical hydrogen production activity *Nanoscale* **6** 13565–71
[7] Sivula K, Le Formal F and Grätzel M 2011 Solar water splitting: progress using hematite (α-Fe_2O_3) photoelectrodes *ChemSusChem* **4** 432–49
[8] Iandolo B, Wickman B, Zorić I and Hellman A 2015 The rise of hematite: origin and strategies to reduce the high onset potential for the oxygen evolution reaction *J. Mater. Chem.* A **3** 16896
[9] Murphy A B, Barnes P R F, Randeniya L K, Plumb I C, Grey I E, Horne M D and Glasscock J A 2006 Efficiency of solar water splitting using semiconductor electrodes *Int. J. Hydrog. Energy* **31** 1999–2017
[10] Bard A J and Fox M A 1995 Artificial photosynthesis: solar splitting of water to hydrogen and oxygen *Acc. Chem. Res.* **28** 141–5
[11] Dias P, Vilanova A, Lopes T, Andrade L and Mendes A 2016 Extremely stable bare hematite photoanode for solar water splitting *Nano Energy* **23** 70–9
[12] Fan Z, Wen X, Yang S and Lu J G 2005 Controlled p- and n-type doping of Fe_2O_3 nanobelt field effect transistors *Appl. Phys. Lett.* **87** 013113
[13] Glasscock J A, Barnes P R F, Plumb I C and Savvides N 2007 Enhancement of photoelectrochemical hydrogen production from hematite thin films by the introduction of Ti and Si *J. Phys. Chem.* C **111** 16477–88
[14] Kay A, Cesar I and Grätzel M 2006 New benchmark for water photooxidation by nanostructured α-Fe_2O_3 films *J. Am. Chem. Soc.* **128** 15714–21
[15] van de Krol R, Liang Y and Schoonman J 2008 Solar hydrogen production with nanostructured metal oxides *J. Mater. Chem.* **18** 2311–20
[16] Jäger S T and Strehle S 2014 Design parameters for enhanced photon absorption in vertically aligned silicon nanowire arrays *Nanoscale Res. Lett.* **9** 511
[17] Bassi P S, Gurudayal, Wong L H and Barber J 2014 Iron based photoanodes for solar fuel production *Phys. Chem. Chem. Phys.* **16** 11834
[18] Mulmudi H K, Mathews N, Dou X C, Xi L F, Pramana S S, Lam Y M and Mhaisalkar S G 2011 Controlled growth of hematite (α-Fe_2O_3) nanorod array on fluorine doped tin oxide: synthesis and photoelectrochemical properties *Electrochem. Commun.* **13** 951–4
[19] Wang G, Gou X, Horvat J and Park J 2008 Facile synthesis and characterization of iron oxide semiconductor nanowires for gas sensing application *J. Phys. Chem.* C **112** 15220
[20] Gurudayal, Chiam S Y, Kumar M H, Bassi P S, Seng H L, Barber J and Wong L H 2014 Improving the efficiency of hematite nanorods for photoelectrochemical water splitting by doping with manganese *Appl. Mater. Interfaces* **6** 5852–9
[21] Kim J Y, Magesh G, Youn D H, Jang J-W, Kubota J, Domen K and Lee J S 2013 Single-crystalline, wormlike hematite photoanodes for efficient solar water splitting *Sci. Rep.* **3** 2681
[22] Kleiman-Shwarsctein A, Hu Y-S, Forman A J, Stucky G D and McFarland E W 2008 Electrodeposition of α-Fe_2O_3 doped

with Mo or Cr as photoanodes for photocatalytic water splitting *J. Phys. Chem.* C **112** 15900–7
[23] Takagi R 1957 Growth of oxide whiskers on metals at high temperature *J. Phys. Soc. Japan* **12** 1212–18
[24] Tallman R L and Gulbransen E A 1968 Dislocation and grain boundary diffusion in the growth of α-Fe_2O_3-whiskers and twinned platelets peculiar to gaseous oxidation *Nature* **218** 1046–7
[25] Fu Y, Chen J and Zhang H 2001 Synthesis of Fe_2O_3 nanowires by oxidation of iron *Chem. Phys. Lett.* **350** 491–4
[26] Fu Y Y, Wang R M, Xu J, Chen J, Yan Y, Narlikar A V and Zhang H 2003 Synthesis of large arrays of aligned a-Fe_2O_3 nanowires *Chem. Phys. Lett.* **379** 373
[27] Wen X, Wang S, Ding Y, Wang Z L and Yang S 2005 Controlled growth of large-area, uniform, vertically aligned arrays of α-Fe_2O_3 nanobelts and nanowires *J. Phys. Chem.* B **109** 215–22
[28] Mema R, Yuan L, Du Q, Wang Y and Zhou G 2011 Effect of surface stresses on CuO nanowire growth in the thermal oxidation of copper *Chem. Phys. Lett.* **512** 87
[29] Wagner R S and Ellis W C 1964 Vapor-liquid-solid mechanism of single crystal growth *Appl. Phys. Lett.* **4** 89
[30] Chernomordik B D, Russell H B, Cvelbar U, Jasinski J B, Kumar V, Deutsch T and Sunkara M K 2012 Photoelectrochemical activity of as-grown, α-Fe_2O_3 nanowire array electrodes for water splitting *Nanotechnology* **23** 194009
[31] Srivastava H, Tiwari P, Srivastava A K and Nandedkar R V 2007 Growth and characterization of α-Fe_2O_3 nanowires *J. Appl. Phys.* **102** 054303
[32] Nasibulin A G, Rackauskas S, Jiang H, Tian Y, Mudimela P R, Shandakov S D, Nasibulina L I, Jani S and Kauppinen E I 2009 Simple and rapid synthesis of α-Fe_2O_3 nanowires under ambient conditions *Nano Res.* **2** 373–9
[33] Grigorescu S, Lee C-Y, Lee K, Albu S, Paramasivam I, Demetrescu I and Schmuki P 2012 Thermal air oxidation of Fe: rapid hematite nanowire growth and photoelectrochemical water splitting performance *Electrochem. Commun.* **23** 59–62
[34] Srivastava H, Tiwari P, Srivastava A K, Rai S, Ganguli T and Deb S K 2011 Effect of substrate texture on the growth of hematite nanowires *Appl. Surf. Sci.* **258** 494–500
[35] Yuan L, Wang Y, Cai R, Jiang Q, Wang J, Li B, Sharma A and Zhou G 2012 The origin of hematite nanowire growth during the thermal oxidation of iron *Mater. Sci. Eng.* B **177** 327–36
[36] Chueh Y-L, Lai M-W, Liang J-Q, Chou L-J and Wang Z L 2006 Systematic study of the growth of aligned arrays of a-Fe_2O_3 and Fe_3O_4 nanowires by a vapor–solid process *Adv. Funct. Mater.* **16** 2243–51
[37] Hiralal P, Saremi-Yarahmadi S, Bayer B C, Wang H, Hofmann S, Wijayantha K G U and Amaratunga G A J 2011 Nanostructured hematite photoelectrochemical electrodes prepared by the low temperature thermal oxidation of iron *Sol. Energy Mater. Sol. Cells* **95** 1819–25
[38] Cornell R M and Schwertmann U 2003 *The Iron Oxides Structure, Properties, Reactions, Occurrences and Uses* 2nd (New York: Wiley-VCH)
[39] Wang R, Chen Y, Fu Y, Zhang H and Kisielowski C 2005 Bicrystalline hematite nanowires *J. Phys. Chem.* B **109** 12245–9
[40] Yuan L, Cai R, Jang J I, Zhu W, Wang C, Wang Y and Zhou G 2013 Morphological transformation of hematite nanostructures during oxidation of iron *Nanoscale* **5** 7581
[41] Zhong D K, Cornuz M, Sivula K, Grätzel M and Gamelin D R 2011 Photo-assisted electrodeposition of cobalt–phosphate (Co–Pi) catalyst on hematite photoanodes for solar water oxidation *Energy Environ. Sci.* **4** 1759–64
[42] Le Formal F, Tétreault N, Cornuz M, Moehl T, Grätzel M and Sivula K 2011 Passivating surface states on water splitting hematite photoanodes with alumina overlayers *Chem. Sci.* **2** 737
[43] Liu Y, Xu Z, Yin M, Fan H, Cheng W, Lu L, Song Y, Ma J and Zhu X 2015 Enhanced photoelectrocatalytic performance of α-Fe_2O_3 thin films by surface plasmon resonance of Au nanoparticles coupled with surface passivation by atom layer deposition of Al_2O_3 *Nanoscale Res. Lett.* **10** 374